Decomposition of Turbulent Velocity Fields in Numerical Simulations of Solar Convection

Nagi N. Mansour[1],Dali Georgobiani[2],Alexander G. Kosovichev[3],Robert F. Stein[4],Åke Nordlund[5]

[1]*NASA Ames Research Center, Moffett Field, CA 94035, USA*

[2]*Center for Turbulence Research, Stanford University / NASA Ames Research Center, Moffett Field, CA 94035, USA*

[3]*Hansen Experimental Physics Laboratory, Stanford University, Stanford, CA 94305, USA*

[4]*Department of Physics and Astronomy, Michigan State University, East Lansing, MI 48824-2320, USA*

[5]*Niels Bohr Institute for Astronomy, Physics and Geophysics, Juliane Maries Vej 30, DK–2100 Copenhagen, Denmark*

ABSTRACT

Velocity fields from simulated solar turbulent convection are investigated by decomposing the vector fields into potential and rotational fields. The motivation for the split is to isolate acoustic fluctuations from turbulent fluctuations, a separation of interest to helioseismology. We associate solenoidal fluctuations with turbulence based on the classical definition that turbulence causes mixing. We analyze both spatial and temporal characteristics of the resulting velocity fields. We find that the energy content is significantly higher in the rotational velocity component, while acoustic mode signatures are in the potential component. These results verify the assumption in helioeismology that the acoustic propagations can be treated using small perturbation analysis.

Subject headings: convection—stars:oscillations—methods:numerical

1. Introduction

Achievements in helioseismic observations, both ground-based (GONG) and space-based (SOHO/MDI), provide large amounts of data about the structure and dynamics of the Sun. These data impose observational constraints on analytical models of turbulent convection, differential rotation, large-scale circulation etc., and are used to test and calibrate these models. In turn, the models are used to understand existing helioseismic observations and predict new effects. Therefore, it is important to develop accurate and realistic models of solar convection and oscillations in order to obtain a clear picture of solar dynamics. The dynamics of the Sun are the major source of space weather that impacts satellite operations and NASA missions. In addition, analytical models verified using solar observations can be applied to other stars (Georgobiani et al. 2004b), and provide predictions of properties of stars, which is the goal of planned NASA asteroseismology missions.

The most realistic models are based on three-dimensional time dependent simulations of solar convection. Simulations of the shallow upper layer of the solar convection zone by Stein & Nordlund (cf Stein & Nordlund (2000) and references therein) demonstrate excellent agreement with existing analytical theories and observations. For instance, comparison of oscillation spectra in the simulated and solar data from SOHO/MDI (cf Georgobiani et al. (2004a)), as well as the rates of stochastic energy input to the low-degree solar modes in the simulations and GOLF observations (Roca Cortés et al. (1999)) show good agreement (see Stein & Nordlund (2001), Fig 7).

Detection and visualization of the particular features of vector fields, namely, their acoustic sources and sinks, as well as their vortices, is very important, because these features affect the physical behavior of flows. However, in the case of turbulent convection flow this is a nontrivial task because turbulence and acoustics are coupled. In this paper, we attempt to investigate properties of turbulent convective flows on the Sun by decomposing them into potential and rotational components. The basic idea is that the potential component contains most of the acoustic field, and the rotational part contains mostly turbulence.

The idea of reconstructing a vector field given its vorticity and divergence dates back to pioneering works of Helmholtz and Kelvin in 1860s. In our days, the formalism of the inverse problem, the decomposition of a given vector field into its potential (curl-free) and vortical (divergence-free) components is widely used in different areas of computational fluid dynamics for feature recognition of the flows. Applications of this formalism can be found in various fields of research, from fluid and deformable object simulations to electromagnetic fields to the analysis of medical data.

The Helmholtz-Hodge decomposition (Abraham et al. 1988) suggests that any smooth vector field can be uniquely represented by the sum of its potential (curl-free), rotational (divergence-free) and harmonic (both curl-free and divergence-free) components. This decomposition helps to extract the flow features and singularities. Technically, the potential flow component contains only sources and sinks, while the rotational term contains only vortices. Discrete analogue of the Helmholtz-Hodge decomposition on regular grids is usually implemented by means of a finite difference approach and is widely used in graphics (see, for instance, Stam 1999; Fedkiw et al. 2001). Amrouche et al. (1998) proposed various methods to solve this issue for piecewise-linear vector fields. Polthier & Preuss (2000) and Polthier & Preuss (2002) derived a variational technique for 2D discrete piecewise-constant vector fields. Based on these works and on Stam (1999), Tong et al. (2003) extended this technique to 3D and combined it with a multiscale vector field decomposition to facilitate feature recognition in vector flows.

The realistic simulations of the convective zone can help to better understand the interactions between mean flow fields, turbulence and acoustics. We use the discrete Helmholtz-Hodge decomposition to analyze the time series of 3D velocity fields from the simulations of solar turbulent convection in an attempt to decouple turbulent and acoustic signals. We decompose a given vector field into potential and rotational components. We analyze the flow features and calculate the spatial and temporal spectra of the potential and rotational components. We find that the kinetic energy content is much higher in the rotational component, while the oscillations are confined in the potential component, although they are driven by turbulence.

2. Velocity Field Decomposition

The goal of this paper is to apply a technique of vector field decomposition to numerical simulations of solar turbulent convection. According to the fundamental theorem of vector analysis, any well-behaved vector field, u_i, has a unique representation, to within constant vectors (harmonic component), as a sum of a potential field, u_i^P, and a solenoidal (rotational) field, u_i^R:

$$u_i = u_i^P + u_i^R, \tag{1}$$

where

$$u_i^P = \phi_{,i};\ u_i^R = \epsilon_{ijk}\psi_{k,j}. \tag{2}$$

Here we use tensor notations for divergence, $\phi_{,i}$, and curl, $\epsilon_{ijk}\psi_{k,j}$. ϵ_{ijk} is the Levi-Civita symbol. For these fields, the following relations hold by definition:

$$\epsilon_{ijk}u_{j,k}^P = 0,\ \epsilon_{ijk}u_{j,k}^R = \epsilon_{ijk}u_{j,k}; \tag{3}$$

$$u_{i,i}^R = 0,\ u_{i,i}^P = u_{i,i}. \tag{4}$$

Roughly speaking, all sources and sinks of a given field u_i are collected in u_i^P, whereas all its vortices appear in u_i^R. This formalism, also called the Helmholtz-Hodge decomposition, is widely used in computational fluid dynamics, because it helps to better visualize complex flows, to recognize their important features, to describe vector fields and study their topology; but it has never been applied before to the 3D numerical simulations of solar convection.

We use the 3D hydrodynamic code by Stein & Nordlund (for details, see Nordlund & Stein 1990; Stein & Nordlund 2000, and references therein) to calculate flow fields in the upper convection zone.

The code simulates the shallow upper layer of the solar convection, 6 Mm by 6 Mm wide and about 3 Mm deep, with a detailed treatment of radiation. We have calculated short series at high resolution, $253\times253\times163$ grid points, and long time series at low resolution, $63\times63\times63$ grid points - 72 hours of solar time, recorded every 30 sec. We use the high resolution fields to study the flow topology, while the low resolution time series of the simulated flow fields are helpful for calculating the spatial and temporal power spectra, energy content of different components etc.

We proceed with the decomposition in the following manner. Without loss of generality, we can split the mean velocity field into a potential and rotational components, according to Eqs (1) - (2):

$$u_i = \epsilon_{ijk}\psi_{k,j} + \phi_{,i} = u_i^R + u_i^P \tag{5}$$

We take divergence of Eq (5):

$$\phi_{,ii} = u_{i,i} = u_{i,i}^P \tag{6}$$

and then solve the resulting Poisson equation on the numerical grid of the code, using its Pade-like finite difference schemes in vertical and horizontal directions, to obtain the potential velocity component. Strictly speaking, the uniqueness of the decomposition requires proper boundary conditions, namely, $u_{i,i}^P$ must be normal to the boundary of the region where the decomposition takes place, while $\epsilon_{ijk}u_{j,k}^R$ must be tangential to that boundary. These conditions reduce to constant u^P and u^R at the boundaries. Constant u^P at the boundaries reflects the fact that the potential component is defined up to a constant. We assume that vorticity is negligible at the boundaries of the simulated domain and substitute the values of the total velocity at the boundaries to solve for the potential component. Then, the rotational component is calculated as a difference between the total velocity and its potential component.

3. Results

Examples of the simulated velocity field and its potential and rotational components are shown as vertical slices through the simulation domain in Fig 1 and as horizontal slices in Fig 2. These results are obtained from the decomposition of the high resolution velocity fields. The total

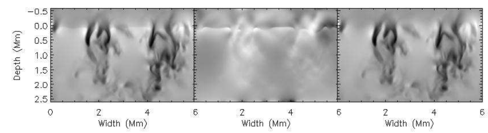

Fig. 1.— Vertical slices of the initial velocity field (left), its potential (middle) and rotational component (right panel) at a fixed arbitrary horizontal coordinate. Potential component looks structureless, while rotational component, similarly to the total velocity, shows strong turbulent downdrafts. The magnitudes change from smallest (light) to largest (dark).

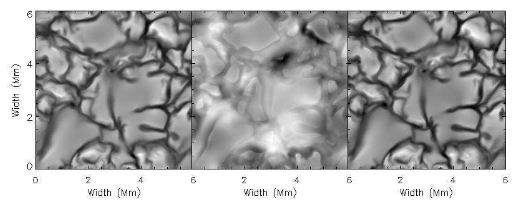

Fig. 2.— Horizontal slices of the initial velocity field (left), its potential (middle) and rotational component (right panel) at the visible surface. There are no sharp features in the potential component, while the rotational component, like the total velocity, exhibits sharp intergranular turbulent features. Black is for largest, white is for smallest magnitudes.

and the rotational velocity slices closely resemble each other visually. From these images, one can conclude that the rotational velocity component is dominant, whereas the potential component is rather weak and featureless. This conclusion is reinforced by the comparison of the time averaged spatial power spectra of the vertical components of these three velocities, measured at the height of 200 km above the visible surface (Fig 3): the energy content is much lower in the potential velocity, and it peaks at lower spatial wavenumber (larger characteristic spatial scale) than the vortical (or total) velocity with its dominant sharp small-scale turbulent features. We also look at the kinetic energy distribution with depth in each of the components (Fig 4). In the region of wave

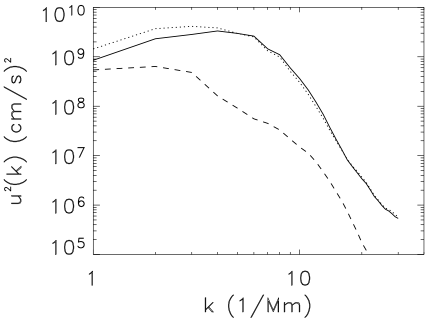

Fig. 3.— Time averaged spatial power spectra of the initial velocity (solid line) and its potential (dashed line) and rotational (dotted line) components at 200 km above the surface. The energy content is much lower in the potential component, and its characteristic spatial scales are larger than for the rotational or total velocities.

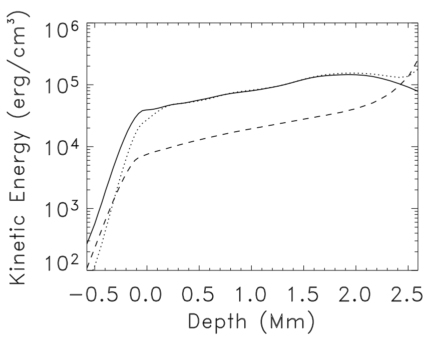

Fig. 4.— Kinetic energy ρu^2 averaged over time and horizontal planes, as function of depth, for the initial velocity (solid line), potential (dashed) and rotational (dotted line) components. The energy is significantly lower in the potential component.

excitation, immediately below the visible surface and down to 1 Mm, the potential component carries significantly less energy than the rotational (or total) velocity.

We construct temporal power spectra of the vertical components for the three velocities, measured at 200 km above the visible surface. Our results show that the potential velocity component displays prominent acoustic modes, whereas the rotational component mostly contributes to the characteristic slope of the background noise, with

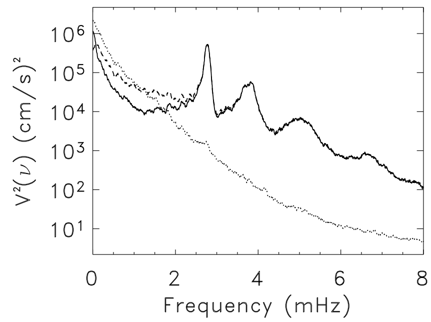

Fig. 5.— Temporal power spectra of different velocity components, measured at 200 km above the surface. Total (solid line) and potential (dashed line) velocity show the oscillation mode peaks; they are very similar, except at low frequencies. Rotational (dotted line) velocity signal represents the background convective noise. The curves are smoothed over $\Delta\nu = 0.1$ mHz.

no mode signal (Fig 5). In this Figure, we plot nonradial power spectra, because the horizontally averaged (radial) rotational velocity component is zero. Both spatial and temporal velocity spectra and their kinetic energies are calculated from the long time series of the low resolution runs. Spatial spectra are averaged over time; kinetic energies of different components are averaged over horizontal planes and time. It is interesting that at low frequencies each component has higher power than the power of the total signal, meaning that these two parts of the velocity field contribute in antiphase.

4. Summary

We have simulated the turbulent velocity field of solar convection using Stein & Nordlund 3D code, and decomposed it into a potential and a rotational component. We have analyzed spatial and temporal spectra of these components. We have found that the kinetic energy content is higher in the rotational velocity component, and that the potential component can be treated as a small perturbation of the total flow field, in agreement with earlier findings (cf Nordlund & Stein 2001). The temporal power spectrum of the potential component shows distinct acoustic mode peaks, while the rotational component spectrum primarily consists of convective background noise, dominating at very low frequencies and quickly decaying at higher frequencies. This suggests that in the potential component, the power is concentrated in the acoustic resonant modes trapped in the upper convection zone.

The velocity field decomposition helps to elucidate the complex problem of the relationship and energy balance between turbulence and oscillations, and to understand the mechanism of generation of acoustic waves by solar and stellar turbulence. Our results show that most of energy is contained in the turbulent component of the flow. Turbulent flows excite acoustic waves, and part of their energy becomes transferred into oscillations. This picture is different from the earlier ideas about the energy equipartition between the turbulent eddies and acoustic modes. Turbulent velocity component exhibits smaller spatial scales than the acoustic component. In a sense, there is a partial inverse cascade, with part of energy being transferred from smaller to larger spatial scales of turbulent convection.

It would be interesting to implement similar velocity decomposition to the simulated velocity fields with higher spatial resolution, and to the simulations with magnetic fields of various geometry and strength; we leave this opportunity for future investigations.

DG is supported by the Center for Turbulence Research. This support is gratefully acknowledged.

REFERENCES

Abraham, R., Marsden, J., & Ratiu, T. 1988, Manifolds, Tensor Analysis, and Applications (Applied Mathematical Sciences, Vol. 75, Springer)

Amrouche, C., Bernardi, C., Dauge, M., & Girault, V. 1998, Math. Meth. Appl. Sci., 21, 823

Asplund, M., Ludwig, H.-G., Nordlund, Å., & Stein, R. F. 2000a, A&A, 359, 669

Asplund, M., Nordlund, Å., Trampedach, R., Allende Prieto, C., & Stein, R. F. 2000b, A&A, 359, 729

Fedkiw, R., Stam, J., & Jensen, H. W. 2001, in Proceedings of ACM SIGGRAPH, 23–30

Georgobiani, D., Stein, R. F., Nordlund, Å., Kosovichev, A. G., & Mansour, N. N. 2004a, in Proceedings of the SOHO14/GONG 2004 Workshop "Helio- and Asteroseismology: Towards a Golden Future"

Georgobiani, D., Trampedach, R., Stein, R. F., Ludwig, H.-G., & Nordlund, Å. 2004b, ApJ, (in preparation)

Hill, F., Fischer, G., Grier, J., et al. 1994, Sol. Phys., 152, 321

Nordlund, Å. & Stein, R. F. 1990, Computer Physics Communications, 59, 119

Nordlund, Å. & Stein, R. F. 2001, ApJ, 546, 576

Polthier, K. & Preuss, E. 2000, in Scientific Visualization, Springer Verlag (Proc. of Eurographics Workshop on Scientific Visualization)

Polthier, K. & Preuss, E. 2002, in Visualization and Mathematics III, Eds: H.C. Hege, K. Polthier, Springer Verlag

Roca Cortés, T., Montañés, P., Pallé, P. L., et al. 1999, in ASP Conf. Ser. 173: Stellar Structure: Theory and Test of Connective Energy Transport, 305

Scherrer, P. H., Bogart, R. S., Bush, R. I., et al. 1995, Sol. Phys., 162, 129

Stam, J. 1999, in Proceedings of ACM SIGGRAPH, 121–128

Stein, R. F. & Nordlund, Å. 2000, Sol. Phys., 192, 91

Stein, R. F. & Nordlund, Å. 2001, ApJ, 546, 585

Tong, Y., Lombeyda, S., Hirani, A., & Desbrun, M. 2003, in Proceedings of ACM SIGGRAPH, 445–452

This 2-column preprint was prepared with the AAS LaTeX macros v5.0.